Nanoscale

RSC Publishing

PAPER

View Article Online
View Journal | View Issue

A novel calix[4]arene thiol functionalized silver nanoprobe for selective recognition of ferric ion with nanomolar sensitivity *via* DLS selectivity in human biological fluid†

Cite this: *Nanoscale*, 2013, **5**, 2364

Alok Pandya, Pinkesh G. Sutariya, Anand Lodha and Shobhana K. Menon*

A high concern for human health and safety has motivated dynamic research on the potential impact of transition metal ions and their toxic effects, thus it is very challenging to design transition-metal ion detection devices that are cost-effective, rapid and applicable to the biological milieus. Driven by the need to detect trace amounts of Fe^{3+} from blood samples, we report a highly selective and ultrasensitive calix[4]arene modified silver nanoprobe for Fe^{3+} recognition at the 9.4 nM level from aqueous solution with excellent discrimination against other heavy metals and biomolecules. The assembly was characterized by TEM (transmission electron microscopy), DLS (dynamic light scattering), UV-Vis, FT-IR, ESI-MS and ^1H NMR spectrometry, which demonstrate the higher binding affinity for Fe^{3+}. The biosensor has been successfully applied to estimate the ferric ion in human blood serum as well as in human hemoglobin.

Received 10th October 2012
Accepted 26th December 2012

DOI: 10.1039/c3nr33119a

www.rsc.org/nanoscale

1 Introduction

Iron metabolism is exquisitely regulated by all organisms from lower species to higher organisms. The various environmental factors which influence growth, such as the availability of nutrients like iron which enhances the physiological activities, profoundly affect gene expression in prokaryotes and are merely important in the metabolism of bacteria in their habitat[1–6] and also play an important role in structural or catalytic functions by enhancing protein and enzymatic activities, biological regulatory aspects and bio-chemical processes at the cellular level in humans[7,8] Thus, the selective detection of biologically important metal ions has gained enormous attention, and sequentially metal ions have been involved in a variety of fundamental environmental and biological processes in organisms. Recently, various fluorogenic and chromogenic chemosensors have been reported to detect biological metal ions such as Hg^{2+}, Zn^{2+}, Ca^{2+}, Cu^{2+} and Pb^{2+}.[9,10] Specifically, Fe acts as a cofactor in many enzymatic reactions involved in the mitochondrial respiratory chain, but its deficiency and excess can induce a variety of diseases.[11,12] Therefore, ferric ion detection has received a great deal of study. Despite the essential role of iron in various fields, selective and sensitive sensors for Fe^{3+} are still uncommon.

Plasmonic nanoparticles (*i.e.* Au and AgNPs) have evolved as one of the most promising current analytical methodologies that arise due to higher enhancement factors, extremely high extinction coefficients and the interparticle distance-dependent optical properties.[13] AuNPs are the preferable candidates for the colorimetric probes owing to their outstanding stability, versatility of modification and high sensitivity of color change, and sensors based on it have been devised for the detection of a broad range of analytes, including metal ions,[14] genes,[15] proteins,[16] inorganic anions,[17] bacteria,[18] and amino acids.[19] Nowadays, the research focus on this issue has been concerned with the use of AuNPs compared to other noble metallic nanoparticles such as silver nanoparticles (AgNPs).[20] This may be due to the chemical degradation of AgNPs under the functionalization conditions and the exposure of the silver surface to oxidation.[21] However, the benefit of using AgNPs rather than AuNPs is that the molar extinction coefficient is 100-fold greater, which increases sensitivity and leads to improved visibility due to the difference in optical brightness.

Recently, we reported potassium ion recognition by benzo-15-crown-5-gold nanoparticles,[22] selective amino acid recognition of lysine, arginine and histidine by functionalized calix[4]arene thiol Au nanoparticles,[23] rapid colorimetric detection of sulfide using calix[4]arene modified gold nanoparticles as a probe[24] and a novel nanoaggregation detection technique of TNT using nanocurcumin as a probe.[25] The sensitivity and selectivity of these sensors prompted us to design and develop sensors, on the same line, for Fe^{3+} ions.

Department of Chemistry, School of Sciences, Gujarat University, Ahmedabad, 380 009, Gujarat, India. E-mail: shobhanamenon07@gmail.com; Fax: +91 79 26308545; Tel: +91 79 26302286

† Electronic supplementary information (ESI) available: Supplementary materials of the synthesis procedure associated with this article can be found. See DOI: 10.1039/c3nr33119a

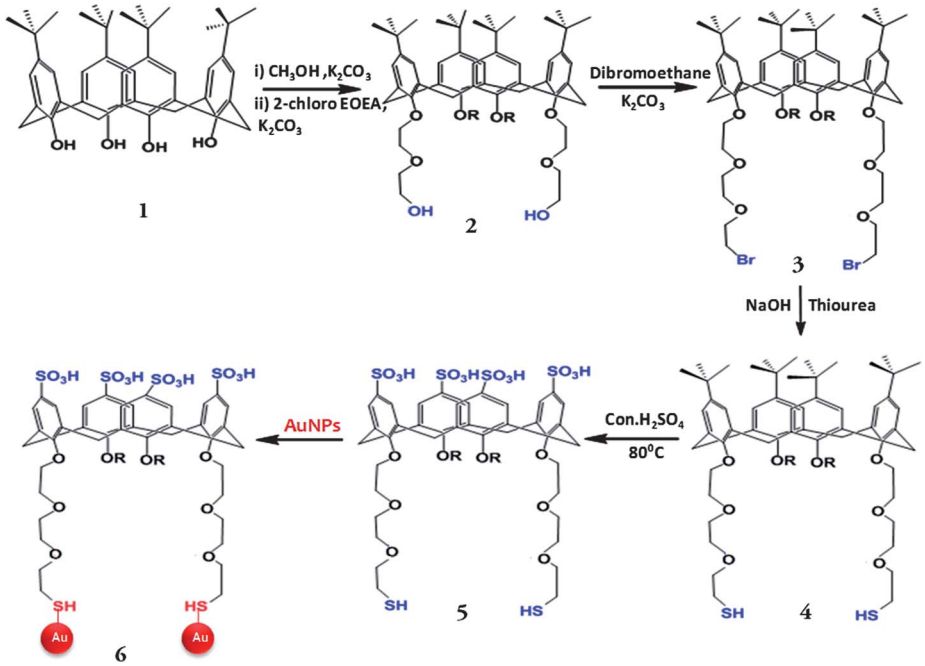

Scheme 1 Synthesis of the *p*-STEC$_4$-AgNP ligand.

Various research groups have worked on FRET based sensors which are created in the form of a dyad or a triad in which the donor and the acceptor are covalently linked through a spacer with a certain length. However, FRET-based sensors can also be created within colloidal nanoparticles, such as capped quantum dots,[26–29] dye doped silica and polymeric nanoparticles,[30–33] and these particle based FRET systems are to be used in biomedical and environmental applications, so it is essential that they are nontoxic and water-soluble to prevent aggregation and precipitation and should have a substantial photoluminescence quantum yield in water. In addition, some rhodamine-based sensors for Fe^{3+} *via* fluorescence enhancement have been reported.[34]

It is well recognized that calixarene has a unique configuration that makes its outer surface hydrophilic and its inner surface hydrophobic and shows excellent selectivity towards guest species, which can be tuned by varying the shape and size of the cavity or by modifying the substituents of the upper and lower rims.[35] Herein, we demonstrate a novel alternative strategy for constructing calix[4]arene modified silver nanoparticles for detection of iron with excellent sensitivity at the nano level and selectivity over the other metals and biomolecules.

In our method, we designed a new promising approach using a Ag nanoparticle based colorimetric sensing system (ANCSS) which forms a calix[4]arene-ethoxythiol functionalized Ag nanoprobe complex (CX-ET-AgNPs) for the detection of ferric ion in water. A closed chamber of a microwave system with precise temperature control function was employed to synthesize the Ag nanoparticles. In the microwave assisted method, the nanomaterial can be selectively heated preferentially in comparison to the solvent and the ligand.[36] This sensor is based on *p*-sulphonato-25,27-bis(triethoxytriethylsulfanyl)-26,28-diethoxy calix[4]arene and Ag nanoparticles (Scheme 1). The silver nanoparticles and *p*-tert-butylcalix[4]arene were synthesized by the microwave assisted method similar to our earlier reported method.[25]

2 Materials and methods

All chemicals used were of analytical grade or of the highest purity available. All solutions were prepared with double-distilled and deionized water. $HAuCl_4$ and soda citrate were purchased from Aldrich. Other biological specimens *i.e.* human hemoglobin, pepsin, cytocrome c, BSA and myoglobin were purchased from Sigma Aldrich with high purity. Silica gel (Merck, 0.040–0.063 mm) was used for column chromatography. Working standard solutions were prepared daily in deionised water. To study the effect of pH, 0.025 M potassium hydrogen orthophosphate (KH_2PO_4) buffer solution was added to 0.2% orthophosphoric acid to get pH from 3.5 to 6.5 and to make basic pH, 0.025 M potassium dihydrogen orthophosphate (KH_2PO_4) buffer solution was added to 0.2% NaOH to maintain the pH between 8 and 12. UV–vis absorption spectra were acquired on a Jasco V-570 UV–Vis spectrophotometer. FT-IR spectra were measured with a Bruker Tensor-27 FT-IR spectrophotometer. Transmission Electron Micrograph (TEM) was recorded on a JEOL, JEM-2100 (200 kV). ^{1}H NMR was carried out in $CDCl_3$ (TMS for internal standard) or DMSO on a Bruker, Avance II (500 MHz). DLS measurements were performed using a Nanotrac instrument. pH measurements were made by using model EQ-664 (Equiptronics).

2.1 *p*-Sulphonato-25,27-bis(triethoxytriethylsulfanyl)-26,28-diethoxy calix[4]arene capped silver nanoparticles (*p*-STEC$_4$-AgNPs), 6

0.25 mM AgNPs were added to 0.1 mM *p*-sulphonato-25,27-bis(triethoxytriethylsulfanyl)-26,28-diethoxycalix[4]arene **5** and were kept stirring for 1 h, resulting in the formation of *p*-sulphonato-25,27-bis(triethoxytriethylsulfanyl)-26,28-diethoxy calix [4]arene capped silver nanoparticles (*p*-STEC$_4$-AgNPs). To evaluate the binding affinity of the Ag–S bond, we carried out FT-IR experiments with *p*-STEC$_4$ and *p*-STEC$_4$-AgNPs. The significant feature (Fig. S1, see ESI†) is the absence of the S–H stretching (2515 cm^{-1}) band which explicitly supports the formation of the Ag–S bond.

2.2 Ferric ion detection using *p*-STEC$_4$ functionalized silver nanoparticles

The stock solution of ferric chloride (0.01 M) was prepared by dissolving ferric chloride (1.62 g) in deionised water and adding a few drops of sulphuric acid to put off hydrolization. Further, it was diluted to the range of 10 nM, 50 nM, 100 nM, 500 nM, 1 μM, 10 μM, and 1 mM and detected by a 0.15 mM solution of *p*-STEC$_4$-AgNPs. To detect Fe^{3+}, 2 ml of 0.1 mM ferric chloride was added to 3 ml of 0.15 mM *p*-STEC$_4$-AgNPs with 2 ml of phosphate buffer of pH 5 and made up to 10 ml. The shift in the SPR absorption maximum of the *p*-STEC$_4$-AgNPs on adding predetermined quantities of Fe^{3+} standard is recorded using a UV-Visible absorption spectrophotometer and a calibration curve was plotted. The fresh human blood samples were collected from a local hospital from healthy subjects.

3 Results and discussion

The surface plasmon resonance makes the absorption cross-section of the nanoparticles several orders of magnitude stronger than the most strongly absorbing molecules. Once the nanoparticles come into proximity with each other, their scattering profiles change, resulting in changes in the color of the solution and the absorption spectra as well. Distinctive colors originating from different degrees of particle aggregation can be readily observed by the naked eye. We investigated spectrophotometrically, the UV visible spectrum of the calix capped Ag nanoparticles solution which shows an absorption maximum at 422 nm (Fig. 1A). Thus, most of the applications of Ag nanoparticles as sensors are based on detecting the shift in the surface plasmon peak either due to change in the local dielectric constant of the nanoparticles by adsorbed molecules or due to analyte induced aggregation of the nanoparticles.[37] Both these effects rely on the selectivity provided by the functionalized capping agent. After long time storage, the calixarene capped Ag nanoparticle surface plasmon band wavelengths remained the same which indicates that microwave synthesized nanoparticles are stable. The calix capped Ag nanoparticles are soluble in water and the clear solution appears pale yellow. Fig. 1a shows the surface plasma resonance and photo images of AgNPs in the absence of ferric ion, *p*-STEC$_4$-AgNPs was pale yellow (a) and displayed an intense surface plasma band at about 422 nm. While in the presence of 100 nM ferric ion, the absorbance of *p*-STEC$_4$-AgNPs at 422 nm decreased and significantly, a new peak appeared at about 554 nm with the color of *p*-STEC$_4$-AgNPs changing from vivid yellow to pale red (b). This broadening and red shifting indicates that the state of *p*-STEC$_4$-AgNPs has changed from mono-dispersed to aggregation (Fig. 1b).

3.1 Sensitive colorimetric detection of ferric ion

The sensitivity of the *p*-STEC$_4$-AgNPs probe toward Fe^{3+} was investigated. Several calibration samples with different concentrations of Fe^{3+} (three measurements for each concentration) were analyzed, and UV-visible absorption spectra were collected. To examine direct colorimetric determination of ferric ion, UV–visible spectra were recorded in the absence and presence of different concentrations of ferric ion.

As we know, the color of 0.15 mM *p*-STEC$_4$-AgNPs was vivid yellow and displayed a characteristic absorption band at 422 nm (Fig. 1A). However, a color change to pale red took place due to aggregation and significant change in the spectral profile was noticed upon the gradual addition of different concentrations of Fe^{3+} from 25 nM to 5 nM with 0.15 mM *p*-STEC$_4$-AgNPs. These changes were due to gradual decrease in the surface plasmon

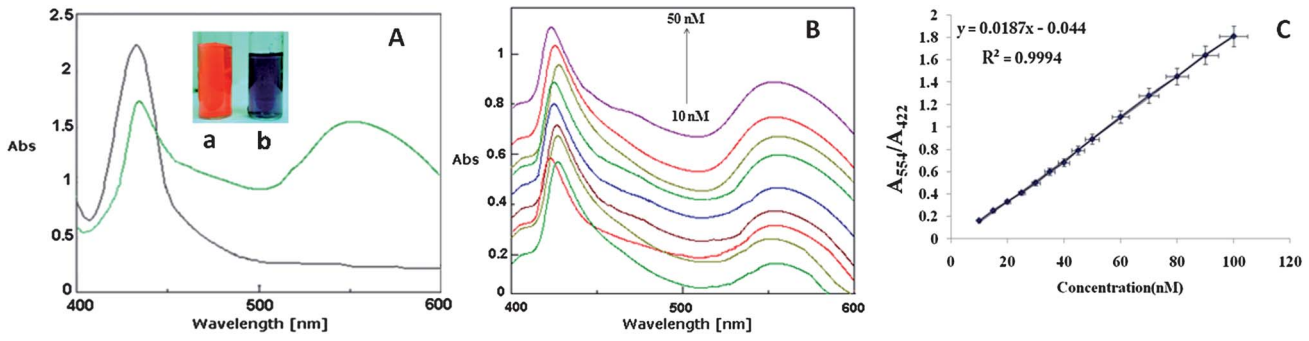

Fig. 1 (A) UV–Vis spectra of (a) *p*-STEC$_4$-AgNPs (b) *p*-STEC$_4$-AgNPs with 100 nM Fe^{3+} concentration. (B) UV-Visible spectra obtained from solutions of 0.15 mM *p*-STEC$_4$-AgNPs responding to various concentrations of Fe^{3+}. The curves from the bottom to top show gradually increasing concentrations of ferric ion: (a) 10 nM, (b) 15 nM, (c) 20 nM, (d) 25 nM, (e) 30 nM, (f) 35 nM, (g) 40 nM, (h) 45 nM, and (i) 50 nM. (C) Linear correlation between absorbance and Fe^{3+} at pH 5.0 adjusted by NaOH–H_3PO_4 buffer, 25 °C.

resonance at about 422 nm and the appearance of a new band at about 554 nm (Fig. 1B) which were ascribed to the aggregation of AgNPs and exhibit selective binding with the ferric ion *via* complexation between the ferric ion with multiple binding sites (p-STEC$_4$-AgNPs–Fe^{3+}). Prominently, it was found that even the addition of trace ferric ion could lead to an obvious color change which could be distinguished with the naked eye. The absorption ratio A_{554}/A_{422} was used to quantify the concentration of ferric ion. It is concluded that the change in the solution color and the degree of red shift are associated with the increase in the size of aggregated nanoparticles (Fig. 1B). However after 5 days the color fades very slowly due to sedimentation. The linear range for Fe^{3+}, using 0.15 mM p-STEC$_4$-AgNPs, is found to be 10 nM–100 nM ($R^2 = 0.999$) (Fig. 1C). The lower detection limit was found to be 9.4 nM. As shown in Fig. S2 (see ESI†) the absorption ratio A_{554}/A_{422} remained unchanged after 4 min, which indicates that the interaction was almost completed under this condition. Therefore, all the absorption measurements were performed in 2 min.

3.2 Dynamic light scattering measurements

To evaluate the aggregation of p-STEC$_4$-AgNPs–Fe^{3+}, we have examined p-STEC$_4$ attached silver nanoparticles using the DLS technique. The dynamic light scattering (DLS) technique illustrates that before surface modification, the nanoparticles had an average hydrodynamic diameter of ~40 nm which maintains their size and stability. After ligand exchange, the p-STEC$_4$ coating on AgNPs, the average hydrodynamic diameter increased to ~52 nm (Fig. 2A1), which is close to the average hydrodynamic diameter of AgNPs. In contrast, upon addition of different concentrations of Fe^{3+} (10 nM and 10 μM), silver nanoparticles agglomerated and their size increased to (~374 nm and ~901 nm) respectively (Fig. 2A2 and A3). Thus, the p-STEC$_4$ conjugated AgNP based DLS assay should be able to show the response at lower concentrations of ferric ion where only smaller aggregates form and at higher concentrations of ferric ion where bigger aggregates form.

3.3 TEM analysis

To appraise the aggregation of p-STEC$_4$-AgNPs–Fe^{3+}, further we have studied p-STEC$_4$ attached silver nanoparticles based TEM measurements. The TEM micrograph for the typical sample resultant from p-STEC$_4$ AgNPs was completely discrete with a mean diameter of ~52 nm (Fig. 2B1). But after the addition of different concentrations (10 nM, 1 μM) of ferric ion to p-STEC$_4$-AgNPs, TEM measurements indicate the formation of p-STEC$_4$-AgNP aggregates due to multiple binding sites of p-STEC$_4$ forming a complex with Fe^{3+} (Fig. 2B2 and B3).

3.4 Effect of pH

We also examined the stability of the p-STEC$_4$-AgNP assembly at different pH conditions (Table S1, see ESI†). It was perceived that p-STEC$_4$-AgNPs exhibited stability with acidic pH solution or basic pH solution using surfactants and remained more stable in the range of pH 4 to 10 for weeks to months with no sign of further aggregation. Furthermore, the p-STEC$_4$-AgNP assembly displays a high stability at room temperature with no sign of aggregation.

We investigated the detection ability of the sensors in buffer solutions with different pH (Fig. 3). At acidic pH, our assay showed sensitive response to Fe^{3+}; large absorption maximum changes were observed in the presence of Fe^{3+}, while our assay

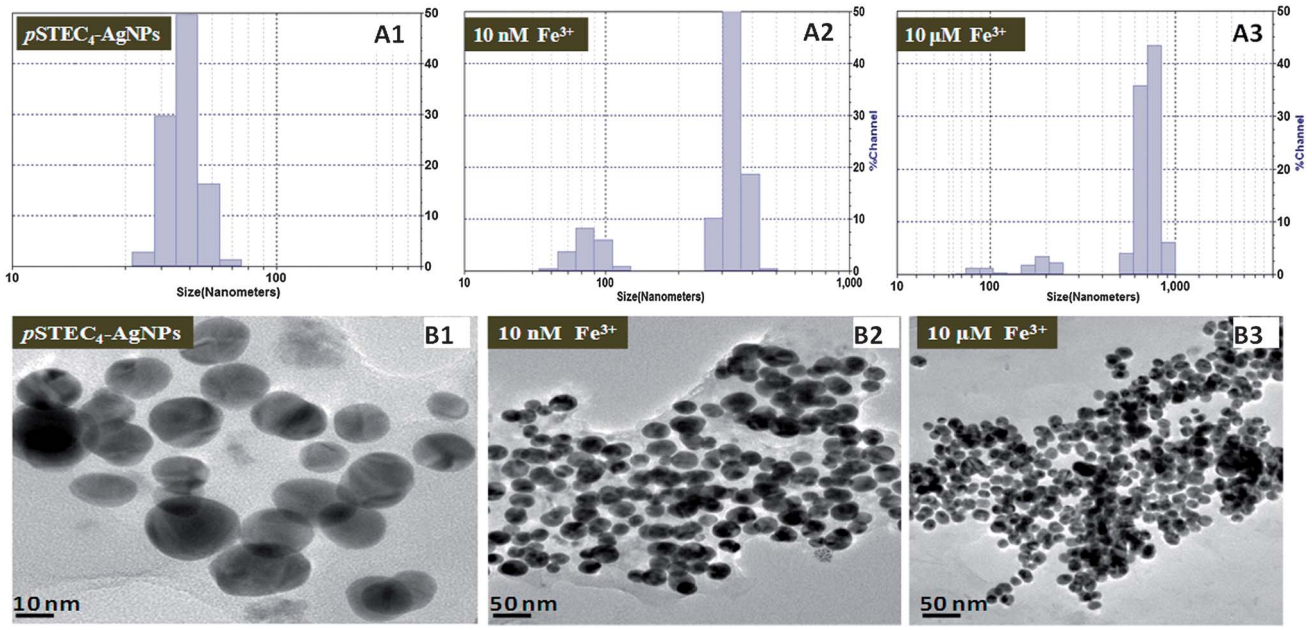

Fig. 2 (A) Size distribution of p-STEC$_4$ conjugated AgNPs measured by DLS. (A1) In the absence of Fe^{3+}, (A2) in the presence of 10 nM Fe^{3+} and (A3) 10 μM Fe^{3+}. (B) TEM images showing how p-STEC$_4$–AgNP aggregate sizes vary in response to the addition of different concentrations of Fe^{3+} (B1) in the absence of Fe^{3+}, (B2) in the presence of 10 nM Fe^{3+} and (B3) 10 μM Fe^{3+}.

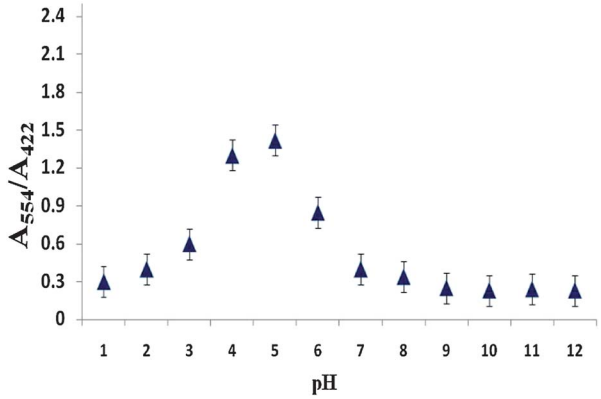

Fig. 3 Plot after the addition of ferric ion to the *p*-STEC$_4$-AgNPs at different pH conditions.

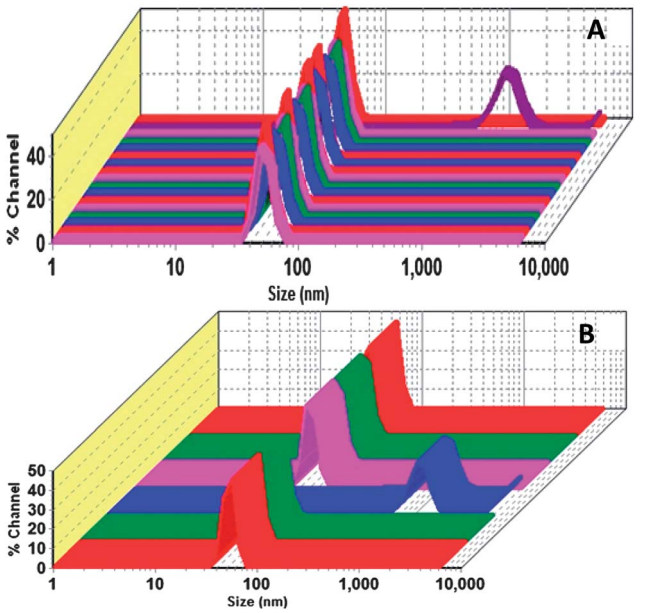

Fig. 4 Size distribution of *p*-STEC$_4$-AgNP solutions after adding (A) 10 μM of different metal ions, Zn^{2+}, Fe^{3+}, Cu^{2+}, Ca^{2+}, Co^{2+}, Mg^{2+}, Cd^{2+}, Ba^{2+}, Na^{+}, K^{+}, Mn^{2+}, Fe^{2+}, Pb^{2+}, Ni^{2+}, Pd^{2+}, and Hg^{2+}, from top to bottom and after adding 10 μl of different biomolecules from top to bottom. (B) Myoglobin, pepsin, BSA, human hemoglobin, cytocrome c, and *p*-STEC$_4$-AgNPs.

did not respond to Fe^{3+} ions sensitively in neutral and basic pH. Unexpectedly, the sensitivity of the sensors to Fe^{3+} seems to be the best at pH 5. Thus, the sensors were expected to have a greater binding affinity to Fe^{3+} at pH 5. However, the solubility of ferric ion decreases at pH >6 with formation of insoluble ferric hydroxides from ferric ion.[38] We suppose that the sensitivity of the sensor is best at pH 5 because the acid group of the sensors is converted to a negatively charged form and the formation of ferric hydroxide is not considerable at pH 5, whereas even though the acid group of the sensors is fully negatively charged, the formation of ferric hydroxide might increase at pH 6, resulting in the decrease of the sensitivity of the sensors at pH 6.

3.5 Selectivity of the assay

The selectivity of this assay approach toward Fe^{3+} was evaluated by absorption spectroscopy and dynamic light scattering (DLS) with other closely related metal ions such as Zn^{2+}, Fe^{3+}, Cu^{2+}, Ca^{2+}, Co^{2+}, Mg^{2+}, Cd^{2+}, Ba^{2+}, Na^{+}, K^{+}, Mn^{2+}, Fe^{2+}, Pb^{2+}, Ni^{2+}, Pd^{2+}, and Hg^{2+} (10 μM) and other biomolecules such as pepsin, cytochrome c, BSA and myoglobin (10 μL) in the presence of 0.15 mM *p*-STEC$_4$-AgNPs. The experimental results were shown in Fig. S3 (see ESI†). It was clear that only Fe^{3+} showed a remarkable higher absorption ratio (A_{554}/A_{422}), confirming the excellent selectivity of the proposed assay to Fe^{3+}. In order to confirm the selectivity, we employ a more sensitive DLS method. As shown in Fig. 4A and B, the size of *p*-STEC$_4$-AgNPs is the largest after treating with Fe^{3+} (10 μM), which indicates that *p*-STEC$_4$-AgNPs have a good selectivity towards Fe^{3+} over the above mentioned metal ions and biomolecules. So, the DLS analysis shows greater selectivity at lower concentration than at high concentration.

3.6 Cation binding mechanism

As we know, supramolecular organizations such as calix[4]arene are ideal frameworks for molecular recognition because of their conformational and structural flexibility and ability to be modified at both the upper and lower rims. Introduction of moieties containing O, N, and S on the calixarene brings the selectivity toward transition metal ions.[39–41] Appropriate functionalization can improve the solubility and can extend its range of applications in the ion and molecular recognition properties of the 1,3-disubstituted derivative of calix[4]arene. Thus, when we investigated spectrophotometrically, experimental observation indicated that the bathochromic shift is observed during interaction of the *p*-STEC$_4$-AgNPs with Fe^{3+} which is due to the existence of the calixarene manifold binding site complex with Fe^{3+}.

When the proof-of-concept experiments were performed, it could be clearly observed from Fig. 5A that for uninteracted 0.1 mM *p*-STEC$_4$ **5** the absorption maximum was observed at 299 nm. But interestingly, after interaction of Fe^{3+} with 0.1 mM *p*-STEC$_4$ the absorption maximum shifted to 310 nm and 357 nm. These observations suggested that the appearance of the new-fangled sharp absorption peak maximum is due to the rapid formation of the *p*-STEC$_4$-AgNPs–Fe^{3+}complex. The simple *p*-tert butyl dibromodiethoxy ethylcalix[4]arene and *p*-tert butyldithiacalix[4]arene do not show any change in the absorption maximum. Additionally, we also evaluated the interaction of AgNPs directly with the ferric ion by UV-Vis spectroscopy which shows a decrease in absorbance and broadened with a small shift in the absorption maximum owing to strong chemisorptions. These results clearly evidence the involvement of *p*-STEC$_4$ for the detection of ferric ion (Fig. 5B).

The binding mechanism of Fe^{3+} with *p*-STEC$_4$ was further evidenced by FT-IR spectroscopy. Fig. 5C shows FT-IR spectra in the region of 4000 to 400 cm^{-1} for both species. The most notable modes from *p*-STEC$_4$ are the C–O stretching band centered at 1072 cm^{-1} with several modes with a C–O stretching component in the 850–1180 cm^{-1} region and the S–H stretching

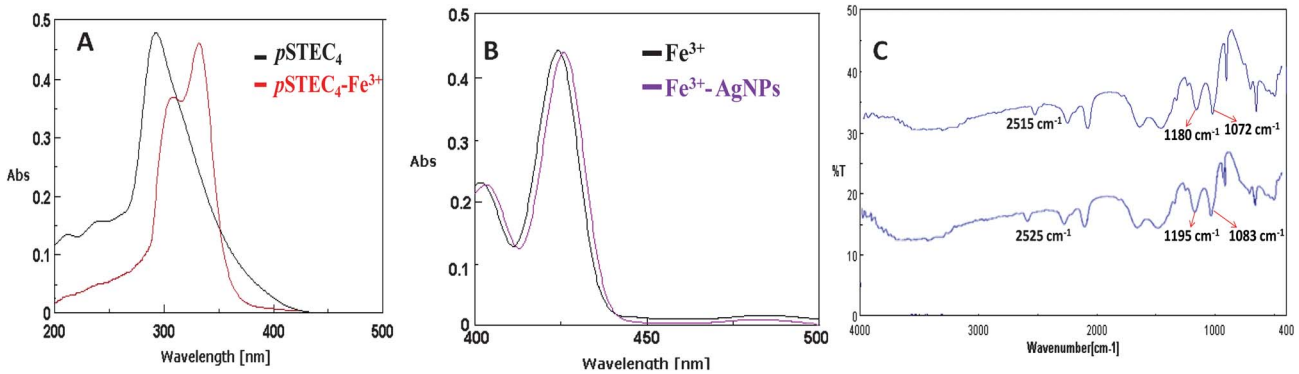

Fig. 5 (A) UV-Vis spectra and (B) UV-Vis spectra of interaction of silver nanoparticles with the ferric ion. (C) FT-IR spectra as a function of interaction of *p*-STEC$_4$ with the ferric ion, pH 5.0 adjusted by NaOH–H_3PO_4 buffer, *T* 2min, 25 °C.

band at 2515 cm^{-1} (Fig. 5C(i)).Then spectra of Fe^{3+} bound to *p*-STEC$_4$ show a slight shift in the C–O stretching band centered at 1083 cm^{-1}, the C–O stretching component in the 1195 cm^{-1} region and, the S–H stretching band at 2525 cm^{-1} (Fig. 5C(ii)). These observations are clear evidence of the formation of the *p*-STEC$_4$–Fe^{3+} complex. Fig. 6 shows the schematics of Fe^{3+} sensing with *p*-STEC$_4$ modified AgNPs *via* nanoaggregation due to specific intramolecular or intermolecular interaction between *p*-STEC$_4$-AgNPs and the ferric ion due to multiple binding sites of *p*-STEC$_4$.

p-STEC$_4$–Fe^{3+} complex formation was further confirmed by ESI-MS spectroscopy. Fig. S4† shows the ESI-MS spectra of the mixtures of *p*-STEC$_4$-AgNPs and Fe^{3+} with *p*-STEC$_4$-AgNPs in aqueous solution. The spectra of *p*-STEC$_4$-AgNPs showed a peak at $m/z = 1094.2$ (Fig. S4A,†). When the ferric ion were mixed with *p*-STEC$_4$-AgNPs in aqueous solution, the *p*-STEC$_4$-AgNPs–Fe^{3+} peak at $m/z = 1145.0$ was clearly detected (Fig. S4B†), which undoubtedly suggests the formation of a complex between multiple binding sites of *p*-STEC$_4$-AgNPs and Fe^{3+}.

4 Detection of ferric ion in human hemoglobin

The analytical application of calix modified silver nanoparticles is demonstrated by applying it to the real analysis of ferric ion in human hemoglobin purchased from Sigma Aldrich with high purity. Then, 1.0 ml of 20% ascorbic acid was added to oxidize the heme solution whilst maintaining the pH between 4 and 5 using phosphate buffer and then the mixture was centrifuged. The supernatant liquid was diluted up to 10, 100, and 1000-fold

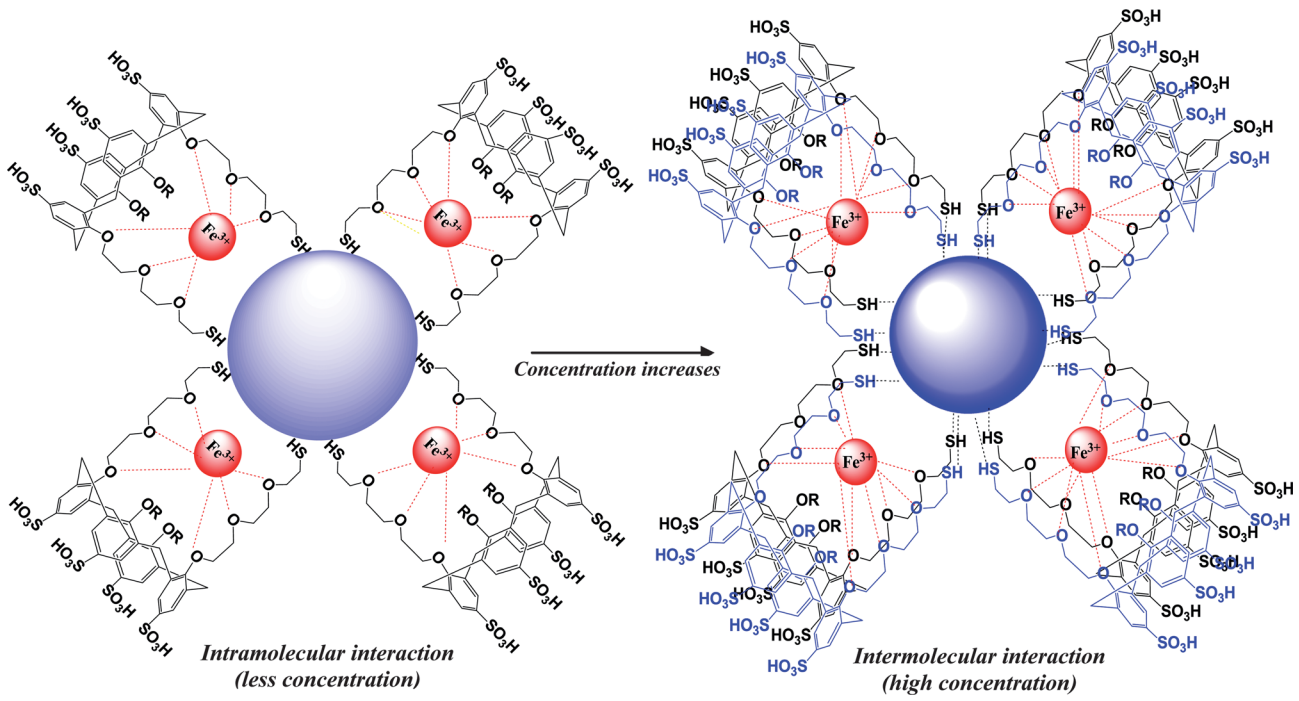

Fig. 6 Schematics of the ferric ion sensing with *p*-STEC$_4$ modified AgNPs *via* nanoaggregation due to specific intramolecular or intermolecular interaction between *p*-STEC$_4$-AgNPs and ferric ion.

Table 1 Determination and recovery of ferric ion in human hemoglobin and blood (BL) samples using the *p*-STEC$_4$-AgNP ferric ion biosensor. (n = three replicates were performed)

Sample	Concentration of Fe by AAS (nM)	*p*-STEC$_4$ capped Ag nanoparticles (nM)	RSD^n (%)	Ferric ion added (nM)	Ferric ion found (nM)	Recovery (%)	RSD^n (%)
Human hemoglobin	96.3	95.2	1.02	20	115.6	98.3	1.32
BL1	81.5	80.2	0.93	20	100.1	99.9	1.23
BL2	76.5	74.8	0.97	20	93.3	98.4	1.78
BL3	66.3	65.4	1.12	20	82.5	96.6	0.92
BL4	68.1	67.9	0.99	20	81.9	93.1	1.13

and analyzed by the presented method and the results are shown in Table 1.The quantitative recovery is found to be 98.3% with a relative standard deviation (RSD) of 1.32, which suggests the precision and repeatability of our assay as well as indicates that no significant interference was encountered with the determination of ferric ion in human hemoglobin after an appropriate dilution of the samples. This result validates the use of calix capped silver nanoparticles in the application of real samples with high sensitivity and specificity.

5 Detection of ferric ion in blood (BL) samples

To exemplify the feasibility of the *p*-STEC$_4$-AgNP based ferric ion biosensor in practical analysis, it was employed to measure ferric ion in human blood. The concentration of ferric ion in human blood is from 8.62 to 11.17 mM L^{-1} for most healthy subjects. Fresh human blood (BL1, BL2, BL3, BL4) samples were collected from a local hospital and analyzed with a *p*-STEC$_4$-AgNP based ferric ion biosensor. In our work, the blood serum samples were simply diluted with maintaining a pH of 5.0. The absorbed ferric ion element was diluted up to 10 and 100-fold and analyzed by the present method and the results are shown in Table 1. The quantitative recovery ranged from 93.1% to 99.9% and the relative standard deviation (RSD) ranged from 1.13 to 1.32, which suggests the precision and repeatability of our assay as well as indicates that no significant interference was encountered with the determination of ferric ion in blood samples after an appropriate dilution of the samples. The analysis and recovery test results of calix capped silver nanoparticles exhibit that the ferric ion biosensor offers an excellent, accurate, fast and precise method for the determination of ferric ion in human blood.

6 Conclusion

We have developed a rapid and sensitive calix[4]arene functionalized silver nanoprobe based system that can selectively detect Fe^{3+} in an aqueous medium. The key to the successful formation of this strategy is multiple binding sites of functionalized calix[4]arene. This sensor shows several advantages over the reported colorimetric ferric ion sensors. It is easy to operate and, most importantly, it exhibits fast response time (<80 s) to ferric ion and has long shelf-life (>4 weeks). The plasmon absorption peak was red-shifted proportionally up to 10 nM ferric ion, and good correlation was obtained between the wavelength shift and the concentration pointing out the feasibility of the method for the quantitative measurement of ferric ion in human body fluid. The developed *p*-STEC$_4$-AgNP based human heme biosensor has been proved to be a simple, reliable and accurate nanoprobe. This method can also indirectly assist the medeco-legal system for the routine investigation process.

Acknowledgements

Financial assistance from UGC, New Delhi is gratefully acknowledged.

References

1 Y. Kubo, M. Yamamoto, M. Ikeda, M. Takeuchi, S. Shinkai, S. Yamagu chi and K. Tamao, *Angew. Chem., Int. Ed.*, 2003, **42**, 2036–2040.
2 M. A. Palacios, Z. Wang, V. A. Montes, G. V. Zyryanov and P. Anzenbacher, Jr, *J. Am. Chem. Soc.*, 2008, **130**, 10307–10314.
3 J. Tolosa, A. J. Zucchero and U. H. F. Bunz, *J. Am. Chem. Soc.*, 2008, **130**, 6498–6506.
4 G. de Ruiter, T. Gupta and M. E. van der Boom, *J. Am. Chem. Soc.*, 2008, **130**, 2744–2745.
5 B. C. Ye and B. C. Yin, *Angew. Chem., Int. Ed.*, 2008, **47**, 8386–8389.
6 M. B. H. Youdim, *Neurotoxic. Res.*, 2008, **14**(1), 45–56.
7 O. K. Fix and K. V. Kowdley, *Hereditary hemochromatosis. Minerva Med.*, 2008, **99**, 605–617.
8 P. Aisen, M. Wessling-Resnick and E. A. Leibold, *Iron metabolism, Curr. Opin. Chem. Biol*, 1999, **3**, 200–206.
9 (*a*) X. Chen, S. W. Nam, M. J. Jou, Y. Kim, S.-J. Kim, S. Park and J. Yoon, *Org. Lett.*, 2008, **10**, 5235–5238; (*b*) X. Zhang, Y. Xiao and X. Qian, *Angew. Chem., Int. Ed.*, 2008, **47**, 8025–8029; (*c*) R. W. Tsien and R. Y. Tsien, *Annu. Rev. Cell Biol.*, 1990, **6**, 715–760.
10 (*a*) E. L. Que, D. W. Domaille and C. J. Chang, *Chem. Rev.*, 2008, **108**, 1517–1549; (*b*) D. W. Domaille, E. L. Que and C. J. Chang, *Nat. Chem. Biol.*, 2008, **4**, 168–175; (*c*) K. M. K. Swamy, S.-K. Ko, S. K. Kwon, H. N. Lee, C. Mao, J.-M. Kim, K.-H. Lee, I. Shin and J. Yoon, *Chem. Commun.*, 2008, 5915–5917; (*d*) E. W. Miller, Q. He and C. Chang, *Nat. Protocol.*, 2008, **3**, 777–783; (*e*) Q. He, E. W. Miller, A. P. Wong and C. J. Chang, *J. Am. Chem. Soc.*, 2006, **128**, 9316–9317.

11 S. Altamura and M. U. Muckenthaler, *J. Alzheim. Dis.*, 2009, **16**, 879–895.
12 L. Silvestri and C. Camaschella, *J. Cell. Mol. Med.*, 2008, **12**, 1548–1550.
13 Z. X. Wang and L. N. Ma, *Coord. Chem. Rev.*, 2009, **253**, 1607–1618.
14 (*a*) C. E. Lisowski and J. E. Hutchison, *Anal. Chem.*, 2009, **81**, 10246–10253; (*b*) S. P. Wu, Y. P. Chen and Y. M. Sung, *Analyst*, 2011, **136**, 1887–1891.
15 W. L. Daniel, M. S. Han, J. S. Lee and C. A. Mirkin, *J. Am. Chem. Soc.*, 2009, **131**, 6362–6363.
16 F. X. Zhang, L. Han, L. B. Israel, J. G. Daras, M. M. Maye, N. K. Ly and C. J. Zhong, *Analyst*, 2002, **127**, 462–465.
17 H. X. Li and L. Rothberg, *Proc. Natl. Acad. Sci. U. S. A.*, 2004, **101**, 14036–14039.
18 (*a*) N. T. K. Thanh and Z. Rosenzweig, *Anal. Chem.*, 2002, **74**, 1624–1628; (*b*) D. Aili, R. Selegard, L. Baltzer, K. Enander and B. Liedberg, *Small*, 2009, **5**, 2445–2452.
19 (*a*) X. X. Li, C. Cao, S. J. Han and S. J. Sim, *Water Res.*, 2009, **43**, 1425–1431; (*b*) S. G. Wang, A. K. Singh, D. Senapati, A. Neely, H. T. Yu and P. C. Ray, *Chem.–Eur. J.*, 2010, **16**, 5600–5606.
20 J. S. Lee, A. K. R. Lytton-Jean, S. J. Hurst and C. A. Mirkin, *Nano Lett.*, 2007, **7**, 2112–2115.
21 H. Wei, C. G. Chen, B. Y. Han and E. K. Wang, *Anal. Chem.*, 2008, **80**, 7051–7055.
22 G. Patel, A. Kumar, U. Pal and S. Menon, *Chem. Commun.*, 2009, 1849–1851.
23 G. Patel and S. Menon, *Chem. Commun*, 2009, 3563–4356.
24 A. Pandya, K. V. Joshi, N. R. Modi and S. K. Menon, *Sens. Actuators, B*, 2012, **168**, 54–61.
25 A. Pandya, H. Goswami, A. Lodha and S. K. Menon, *Analyst*, 2012, **137**, 1771–1774.
26 X. Guo, D. Zhang, Y. Zhou and D. Zhu, *J. Org. Chem.*, 2003, **68**, 5681–5687.
27 I. L. Medintz, H. T. Uyeda, E. R. Goldman and H. Mattoussi, *Nat. Mater.*, 2005, **4**, 435–446.
28 I. L. Medintz, S. A. Trammell, H. Mattoussi and J. M. Mauro, *J. Am. Chem. Soc.*, 2004, **126**, 30–31.
29 M. Tomasulo, S. Giordani and F. M. Raymo, *Adv. Funct. Mater.*, 2005, **15**, 787–793.
30 E. Brasola, F. Mancin, E. Rampazzo, P. Tecilla and U. Tonellato, *Chem. Commun.*, 2003, 3026–3027.
31 S. R. Corrie, G. A. Lawrie and M. Trau, *Langmuir*, 2006, **22**, 2731–2737.
32 R. M. Renault, A. Herault, J. J. Vachon, R. B. Pansu, S. A. Gerbier and C. Larpent, *Photochem. Photobiol. Sci.*, 2006, **5**, 300–310.
33 F. Gouanve, T. Schuster, E. Allard, R. M. Renault and C. Larpent, *Adv. Funct. Mater.*, 2007, **17**, 2746–2756.
34 K. S. Moon, Y.-K. Yang, S. Ji and J. Tae, *Tetrahedron Lett.*, 2010, **51**, 3290–3293.
35 R. Joseph and C. P. Rao, *Chem. Rev.*, 2011, **111**, 4658–4702.
36 J. A. Gerbec, D. Magana, A. Washington and G. F. Strouse, *J. Am. Chem. Soc.*, 2005, **127**, 15791–15800.
37 K. Aslan, J. R. Lakowicz and C. D. Geddes, *Anal. Biochem.*, 2004, **330**, 145–155.
38 (*a*) G. S. Baldwin, *Med. Hypotheses*, 1992, **38**, 70; (*b*) G. S. Baldwin, C. Curtain and W. H. Sawyer, *Biochemistry*, 2001, **40**, 10741.
39 A. Ikeda and S. Shinkai, *Chem. Rev.*, 1997, **97**, 1713.
40 C. Redshaw, *Coord. Chem. Rev.*, 2003, **244**, 45.
41 (*a*) M. F. Mahon, J. McGinley, A. D. Rooney and J. M. D. Walsh, *Tetrahedron*, 2008, **64**, 11058; (*b*) J. Sun, D. M. Liu, J. X. Wang and C. G. Yan, *J. Inclusion Phenom. Macrocyclic Chem.*, 2009, **64**, 317.